Dalton Transactions

PAPER

View Article Online
View Journal | View Issue

Cite this: *Dalton Trans.*, 2026, **55**, 2691

Tuning reactivity through implementation of the HSAB concept in oxygen- and sulphur-bridged Al/P and Ga/P FLPs

Julian Buth, [a] Yury V. Vishnevskiy, [a,b] Jan-Hendrik Lamm, [a] Beate Neumann,[a] Hans-Georg Stammler [a] and Norbert W. Mitzel *[a]

Received 20th January 2026,
Accepted 20th January 2026

DOI: 10.1039/d6dt00151c

rsc.li/dalton

Sulphur-bridged frustrated Lewis pairs (FLPs) of the type Bis_2E-S-P$^tBu_2$ (**ESP**; E = Al, Ga) were synthesised in analogy to their oxygen-bridged E–O–P analogues (**EOP**). An exchange reaction between **AlSP** and **GaOP** affords selectively and in accordance with the concept of *hard and soft acids and bases* (HSAB) the inverted systems **AlOP** and **GaSP**. Reactivity studies towards small molecules, such as CO_2, CS_2, SO_2, N_2O, and propylene sulphide, revealed differences in adduct formations. The adducts **EXP**·CX_2 and **EXP**·SO_2 (X = O, S) consist of five-membered heterocycles. The oxidation products **EXP**·X are four-membered rings; they result from the reaction of the **EXP** with N_2O and/or propylene sulfide (under loss of propene), except the reaction of **AlSP** with propylene sulfide that forms a six-membered ring with the whole substrate molecule. The FLP **GaSP** is exceptional because the formation of its CO_2 adduct is temperature-dependent, confirmed by variable-temperature NMR studies, and its adduct **GaSP**·CS_2 has two structural isomers. All CS_2 adducts impress with different colours in solution.

Introduction

With the concept of *hard and soft acids and bases* (HSAB) Ralph G. Pearson defined simple, but reliable rules for interactions between different categories of Lewis acids (LA) and bases (LB).[1] The classification into 'hard' and 'soft' particles, depending on their orbital characteristics, charge density, polarizability, and electronegativity adds a qualitative, predictive power to Lewis theory, especially for stability and direction of reactions. For instance, palladium recycling has recently been improved by applying this principle and exploiting the strong HSAB affinity of Pd^{2+} ions for S^{2-} species in the active site of a capture material.[2]

In view of the increased demand for metal-free catalysts and the discovery of frustrated Lewis pairs (FLPs) with unique reactivity by Douglas W. Stephan in 2006, research in this area has continuously attracted interest.[3–5] Different intra-, intermolecular and hidden FLPs have been developed, featuring various LA/LB element combinations and substituents.[6–16] As limited reversibility has hindered broader catalytic applications, careful tuning of Lewis acidity and basicity is crucial to achieve the necessary balance between reactivity and turnover.

Modulation of the linker moiety in intramolecular systems allows adjusting the strength of the Lewis acidity.[17,18] Comparing CO_2 adducts of methylene- and oxygen-bridged $(C_2F_5)_3$SiX-P$^tBu_2$ FLPs (X = CH_2, O), shows that the electron density donated by the oxygen atom entails a temperature-dependent equilibrium, while the CH_2-spacer leads to an irreversible adduct.[13,19] Other donating linker units consist of nitrogen atoms, for example Al- and Ga-hydrazides, which are easily accessible *via* hydrometallation of hydrazones.[20,21] Further, we synthesised chalcogen-bridged Sb/P systems and their formal HCl adducts.[16]

Recently, we described oxygen-bridged FLPs of the type Bis_2EOP$^tBu_2$ (**EOP**, Bis = $CH(SiMe_3)_2$, E = Al, Ga) based on aluminium and gallium with a focus on their reactivity towards hydrogen (Scheme 1).[22] While both systems split hydrogen, **AlOP** is capable of reducing CO_2 to the formate stage in two successive steps.[23] For the gallium analogue we found a dynamic temperature-dependent equilibrium of the hydrogen adduct $Bis_2Ga(H)OP(H)^tBu_2$ (**GaOP**·H_2), separating to free Bis_2GaH and phosphane oxide at higher temperatures.[22] Beyond small molecule activation and adduct formation, the controlled release of bound species remains essential for enabling catalysis with FLPs. In this work, we implemented the HSAB concept to tune reactivity towards small molecules of oxygen- and sulphur-bridged Al/P and Ga/P FLPs.

[a]*Lehrstuhl für Anorganische Chemie und Strukturchemie, Centrum für Molekulare Materialen CM2, Fakultät für Chemie, Universität Bielefeld, Universitätsstraße 25, Bielefeld 33615, Germany. E-mail: mitzel@uni-bielefeld.de*
[b]*Department of Chemistry, M. V. Lomonosov Moscow State University, Leninskie Gory 1–3, Moscow 119991, Russia*

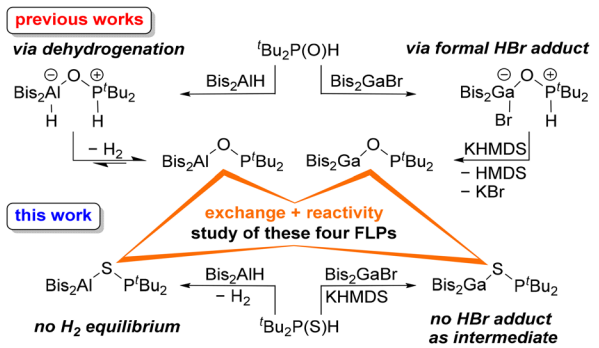

Scheme 1 Synthetic routes to $Bis_2AlOP^tBu_2$ and $Bis_2AlSP^tBu_2$ *via* dehydrogenation from Bis_2AlH, and the one-pot synthesis *via* the formal HBr adduct to $Bis_2GaOP^tBu_2$ or without previous adduct formation to $Bis_2GaSP^tBu_2$ with KHMDS ($KN(SiMe_3)_2$).

Results and discussion

In analogy to the synthesis of $Bis_2AlOP^tBu_2$ (**AlOP**),[23] we reacted Bis_2AlH with the phosphane sulphide $^tBu_2P(S)H$ to afford the sulphur-bridged $Bis_2AlSP^tBu_2$ (**AlSP**) in a dehydrogenation reaction (Scheme 2). Synthetic access to $Bis_2GaSP^tBu_2$ (**GaSP**) was achieved by reacting the gallium bromide Bis_2GaBr with $^tBu_2P(S)H$ followed by deprotonation and salt elimination reaction with potassium hexamethyldisilazanide (KHMDS) – also in analogy to its oxygen-bridged counterpart **GaOP**.

The free **ESP** systems were isolated (**AlSP**: quantitative; **GaSP**: 96%) and fully characterised using NMR spectroscopy, elemental analysis, and single crystal X-ray diffraction experiments. The ^1H NMR spectra show that both FLPs exhibit similar shifts and coupling constants for the doublet of the *tert*-butyl groups: 1.24 ppm ($^3J_{P,H}$ = 11.6 Hz) for **AlSP** and 1.27 ppm ($^3J_{P,H}$ = 11.5 Hz) for **GaSP**. The methine protons were detected at 0.27 ppm (**AlSP**) and 1.06 ppm (**GaSP**), respectively, both strongly downfield-shifted compared to their oxygen-bridged FLP analogues (**AlOP**: −0.38 ppm; **GaOP**: 0.53 ppm). Likewise, the $^{31}P\{^1H\}$ NMR spectra display equal singlets at 69.2 ppm (**AlSP**) and 68.5 ppm (**GaSP**), whereas the corresponding **EOP** systems exhibit far greater downfield shifts (**AlOP**: 142.6 ppm; **GaOP**: 143.5 ppm).

The solid-state structures of the free FLPs **ESP** show trigonal planar coordinated aluminium or gallium atoms, respectively (Fig. 1). Both structures have similar E⋯P distances as well as E–S and S–P bond lengths, while the latter are found to be longer than in $^tBu_2P(S)H$ (1.967(1) Å).[24] The E–S–P angles are identical (**AlSP**: 106.3(1)°; **GaSP**: 106.1(1)°) and vastly narrower than the E–O–P angles (**AlOP**: 138.1(1)°; **GaOP**: 126.2(2)°).

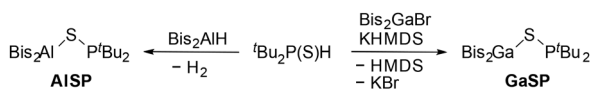

Scheme 2 Synthesis of the sulphur-bridged systems **AlSP** *via* dehydrogenation and **GaSP** *via* deprotonation and salt elimination from di-*tert*-butylphosphane sulphide.

In contrast to the synthesis of **AlOP**, the dehydrogenation to **AlSP** is fast and irreversible. No signals for the H_2 adduct **AlSP**·H_2 were detected, even under hydrogen atmosphere. Contrary to the established procedure for the oxygen-bridged systems **EOP**, no adduct formation to a formal intermediate HBr adduct $Bis_2Ga(Br)\cdot SP(H)^tBu_2$ (**GaSP**·HBr) was observed. Even though an interaction should be favoured, according to the HSAB concept, the signals of Bis_2GaBr and $^tBu_2P(S)H$ are both present in the ^1H NMR spectrum. Presumably the relatively low Lewis acidity and basicity of both components prevent the adduct formation. Using the more Lewis acidic Bis_2AlBr instead, the formal HBr adduct **AlSP**·HBr is afforded in quantitative yield. The proton NMR spectrum shows a doublet at 6.02 ppm with a $^1J_{P,H}$ coupling constant of 445 Hz, which is downfield-shifted and wider than in free $^tBu_2P(S)H$ (5.51 ppm; $^1J_{P,H}$ = 415 Hz). Similarly, the methine proton resonance at −0.41 ppm indicates a tetra-coordinated aluminium atom compared to the tri-coordinate one in the free **AlSP** system (0.27 ppm). The shifts and coupling constants are in line with those of the oxygen-bridged HBr adducts **EOP**·HBr.[22]

The determination of the molecular structure of **AlSP**·HBr in the crystalline state confirmed the tetrahedral environment at the aluminium atom (Fig. 1). The Al⋯P distance and the Al–S bond are longer, while the S–P bond is shorter than in the free FLP **AlSP**. In addition to a wider Al–S–P angle for **AlSP**·HBr, these trends are congruent to the **EOP**/**EOP**·HBr systems. However, in contrast to the oxygen-bridged HBr adducts, it is noticeable that the H⋯Br distance with 2.75(2) Å is less than the sum of the van der Waals radii (3.06 Å).[25] Furthermore, the torsion angle τ(Br–Al–P–H) of **AlSP**·HBr is 3.7(8)° and suggests an attractive H⋯Br interaction as well, which is significantly lower than in the **EOP**·HBr adducts (**AlOP**·HBr τ = 56.1(5)°; **GaOP**·HBr τ = 71.6(8)°). Possibly, this HBr-contact stabilises the **AlSP**·HBr adduct and is a further factor, why the aluminium containing system forms this adduct in contrast to its gallium analogue.

Strikingly, the reaction of **AlSP** and **GaOP** yielded an exchange to **AlOP** and **GaSP**, which is in accordance with the HSAB concept (Scheme 3). Classifying aluminium and oxygen atoms as 'hard' and gallium and sulphur atoms as 'soft' in this context, this exchange benefits from the favoured 'hard–hard' and 'soft–soft' interactions. Monitoring this selective exchange $^{31}P\{^1H\}$ NMR spectroscopically, full conversion was achieved within 48 h (Fig. 2). Furthermore, the same tendency was observed, when adding $^tBu_2P(S)H$ to **GaOP**, which results in the formation of $^tBu_2P(O)H$ and the **GaSP** system. We calculated the thermodynamics of both exchange reactions and confirmed the experimental outcome. **GaOP** + **AlSP** → **GaSP** + **AlOP** results in an energy gain of −10.0 kcal mol^{-1} and **GaOP** + $^tBu_2P(S)H$ → **GaSP** + $^tBu_2P(O)H$ yields −1.9 kcal mol^{-1} (for more details see Table S5 in the SI).

A series of investigations were conducted with the objective of ascertaining the reactivity of the free FLPs towards a range of small molecules, including CO_2, CS_2, and SO_2 (Scheme 4). All isolated adducts were fully characterised by means of NMR spectroscopy, elemental analyses and single crystal X-ray diffraction experiments.

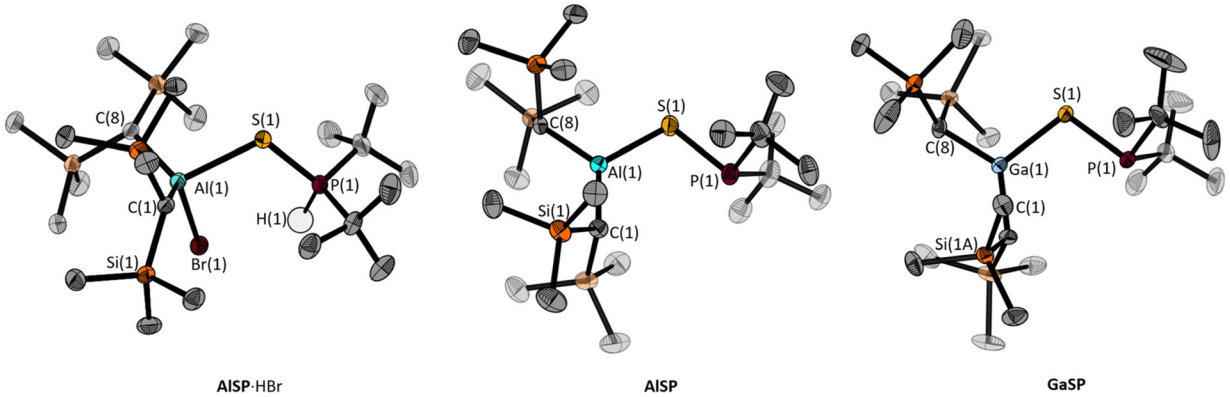

Fig. 1 Molecular structures of **AlSP**·HBr, **AlSP** and **GaSP** in the solid-state. Hydrogen atoms, except of P–H, and minor occupied parts are omitted for clarity. Ellipsoids are set at 50% probability level. Selected distances, bond lengths [Å] and angles [°]: **AlSP**·HBr: Al(1)···P(1) 3.714(1), H(1)···Br(1) 2.75 (2), Al(1)–S(1) 2.451(1), S(1)–P(1) 2.008(1); Al(1)–S(1)–P(1) 112.5(1), C(1)–Al(1)–C(8) 120.6(1), C(1)–Al(1)–S(1) 100.8(1), C(8)–Al(1)–S(1) 107.7(1); **AlSP**: Al(1) ···P(1) 3.464(1), Al(1)–S(1) 2.203(1), S(1)–P(1) 2.126(1); Al(1)–S(1)–P(1) 106.3(1), C(1)–Al(1)–C(8) 127.6(1), C(1)–Al(1)–S(1) 121.3(1), C(8)–Al(1)–S(1) 111.1(1); **GaSP**: Ga(1)···P(1) 3.482(1), Ga(1)–S(1) 2.236(1), S(1)–P(1) 2.121(1); Ga(1)–S(1)–P(1) 106.1(1), C(1)–Ga(1)–C(8) 129.6(1), C(1)–Ga(1)–S(1) 119.5(1), C(8)–Ga (1)–S(1) 110.9(1).

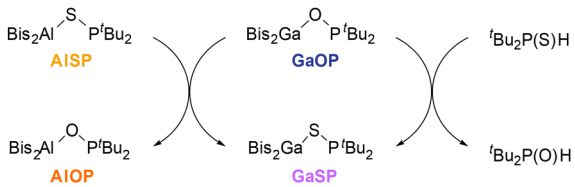

Scheme 3 Exchange reactions of the oxygen- and sulphur-bridged systems **GaOP**/**AlSP** to **AlOP**/**GaSP** as well as **GaOP**/^{t}Bu$_2$P(S)H to **GaSP**/^{t}Bu$_2$P(O)H.

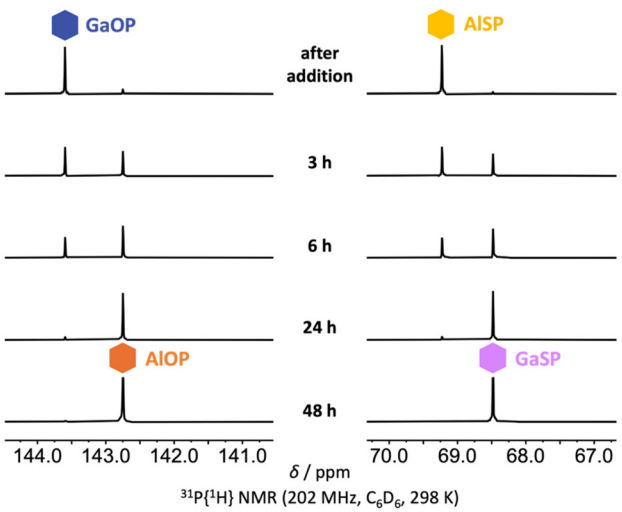

Fig. 2 Sections of the $^{31}P\{^1H\}$ NMR spectra of the exchange reaction between the oxygen- and sulphur-bridged systems **GaOP**/**AlSP** and **AlOP**/**GaSP** in C_6D_6.

Starting with carbon dioxide, adduct formation with CO_2 to **EXP**·CO_2 was observed for all systems. This was confirmed spectroscopically by $^{13}C\{^1H\}$ NMR measurements, with the characteristic doublet for the CO_2 unit at 167.2 ($^1J_{P,C}$ = 98.5 Hz)

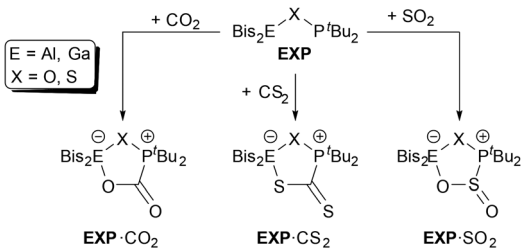

Scheme 4 Reactions of **EXP** with carbon dioxide, carbon disulfide, and sulphur dioxide to their corresponding adducts with five-membered rings.

for **GaOP**·CO_2, 163.3 ($^1J_{P,C}$ = 79.0 Hz) for **AlSP**·CO_2 and 164.2 ($^1J_{P,C}$ = 75.1 Hz) for **GaSP**·CO_2, respectively. In all cases the methine proton resonance and the $^{31}P\{^1H\}$ NMR signal shift strongly towards higher field and the coupling constants of the *tert*-butyl group become larger compared to the free **EXP** systems (Table 1). Whereas **GaOP**·CO_2 and **AlSP**·CO_2 were isolable solids, like the previously reported **AlOP**·CO_2,[23] the **GaSP**·CO_2 adduct is in an equilibrium with free **GaSP** plus CO_2 and only the free FLP was obtained in the residue after drying under reduced pressure. Under CO_2 atmosphere (1 bar) and 298 K in a closed Young NMR tube, the ratio of free **GaSP** and adduct **GaSP**·CO_2 is about 1 : 8, as determined by integration of the ^1H NMR signals. Variable temperature (VT) NMR measurements in the range between 253 and 373 K confirm the reversibility (Fig. 3). At 273 K and below, the equilibrium shifts completely to the side of the adduct **GaSP**·CO_2, and no observable signal for **GaSP** remains in the $^{31}P\{^1H\}$ NMR spectrum. Heating to 373 K, results in the release of CO_2 and the recovery of the free **GaSP**. With higher temperatures, also a gradual downfield shift is observed. Minor impurities with ^{t}Bu$_2$P(S)H, due to hydrolysis, are subject to the same trend. Additionally, quantum chemical calculations of the Gibbs free

Table 1 ^{1}H, $^{13}C\{^{1}H\}$, and $^{31}P\{^{1}H\}$ NMR spectroscopy data of **EXP**·CO_2, **EXP**·CS_2 and **EXP**·SO_2 adducts

	^{1}H (EC**H**)/ppm	^{1}H (^{t}Bu)/ppm	$^{13}C\{^{1}H\}$ (P**C**X_2)/ppm	$^{31}P\{^{1}H\}$/ppm
GaOP·CO_2	−0.35	1.06 ($^{3}J_{P,H}$ = 15.1 Hz)	167.2 ($^{1}J_{P,C}$ = 98.5 Hz)	57.1
AlSP·CO_2	−0.79	1.05 ($^{3}J_{P,H}$ = 16.8 Hz)	163.3 ($^{1}J_{P,C}$ = 79.0 Hz)	73.3
GaSP·CO_2	−0.27	1.13 ($^{3}J_{P,H}$ = 16.4 Hz)	164.2 ($^{1}J_{P,C}$ = 75.1 Hz)	67.9
GaOP·CS_2	−0.17	1.14 ($^{3}J_{P,H}$ = 14.9 Hz)	237.8 ($^{1}J_{P,C}$ = 42.4 Hz)	63.5
AlSP·CS_2	−0.59	1.14 ($^{3}J_{P,H}$ = 16.5 Hz)	232.7 ($^{1}J_{P,C}$ = 18.3 Hz)	91.9
GaSP·CS_2	−0.12	1.19 ($^{3}J_{P,H}$ = 16.3 Hz)	233.0 ($^{1}J_{P,C}$ = 16.2 Hz)	91.7
GaOP·SO_2	−0.31, −0.03	0.87/1.21 ($^{3}J_{P,H}$ = 14.5/15.1 Hz)	—	88.1
AlSP·SO_2	−0.69, −0.57	0.89/1.18 ($^{3}J_{P,H}$ = 16.3/16.4 Hz)	—	117.0
GaSP·SO_2	−0.08	1.07 (br. s)	—	114.9

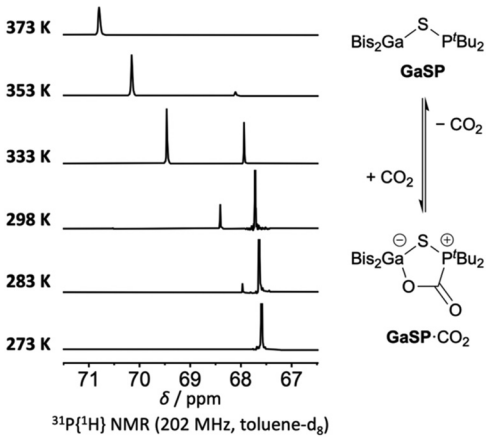

Fig. 3 Details of the $^{31}P\{^{1}H\}$ VT NMR spectra of **GaSP** under CO_2 atmosphere (1 bar) recorded in the range between 273 and 373 K in toluene-d_8.

energy ($\Delta G^{\circ}_{298} = -0.7\,\mathrm{kcal\,mol^{-1}}$) verifies the experimental observed equilibrium.

Using carbon disulfide instead, an adduct formation to **EXP**·CS_2 was achieved. Similar to the CO_2 adducts **EXP**·CO_2, the carbon atom of the CS_2 unit in **EXP**·CS_2 show a low field shift in the $^{13}C\{^{1}H\}$ NMR spectra (232.7–237.8 ppm) compared to free CS_2 (192.7 ppm)[26] and is split into a doublet due to the $^{1}J_{P,C}$-coupling (Table 1). Expectedly, the methine proton resonances of **EXP**·CS_2 show a weaker downfield shift ($\Delta\delta$ = 0.15–0.20 ppm) than in **EXP**·CO_2.

Interestingly, the colours of the adduct solutions range from blue (**GaOP**·CS_2) over green (**AlSP**·CS_2) to yellow (**GaSP**·CS_2), while the obtained crystals were all violet (see Fig. S1 in the SI). UV/vis spectroscopic analyses show single, isolated absorption bands for **GaOP**·CS_2 (λ_{max} = 589 nm) and **AlSP**·CS_2 (λ_{max} = 613 nm), while for **GaSP**·CS_2 two shoulders indicate two species (Fig. S90/S91, SI). TD-DFT calculations suggest that mainly HOMO → LUMO transitions induce the colouring, while in the CO_2 adducts this transition is shifted into the non-visible area (see SI).

Moreover, the reactivity of **GaSP** towards CS_2 is special and results in a mixture of two species. Beside the already mentioned 'classical' adduct with Ga–S–C–P connectivity, another similar set of signals is observed. Due to the further low-field shift of the CS_2 unit ($^{13}C\{^{1}H\}$ NMR: 255.8 ppm), the absence of a P,C-coupling, a signal at 97.1 ppm in the $^{31}P\{^{1}H\}$ NMR spectrum, and the results of the elemental analyses we suggest it to be an isomer. The ratio of 'classical' to 'inverted' adduct is approximately 2.6 : 1.0. The 'inverted' adduct with Ga–C–S–P connectivity matches with the NMR data. Although the calculated thermodynamics for this adduct **GaSP**·S_2C is +22.2 kcal mol^{-1} higher than the 'classical' adduct **GaSP**·CS_2. Further, we optimised acyclic structures and those of a hypothetical six-membered motif plus its dimerisation, whereas the latter is indeed energetically favoured (see SI). However, diffusion-ordered spectroscopy (DOSY) NMR measurements show that both species have similar diffusion coefficients, which contradicts these considerations. Additionally, attempts to calculate a hypothetical four-membered ring adduct failed to converge.

By reacting the **EXP** systems with sulphur dioxide, and contrary to the partial decomposition with **AlOP**,[19] stable adducts were isolated for all three analogues **EXP**·SO_2. All resonances in the ^{1}H NMR spectra for **GaOP**·SO_2 and **AlSP**·SO_2 are split, presumably due to the chirality at the sulphur atom. For **GaSP**·SO_2 extremely broad resonances were detected, especially in the $^{13}C\{^{1}H\}$ NMR spectrum for the methine and the *tert*-butyl group.

Crystal structure determinations of the isolated CO_2, CS_2, and SO_2 adducts of the **EXP** FLPs, confirm five-membered rings with an exocyclic oxygen or sulphur atom, respectively (Fig. 4). In all cases the environment of the Lewis acidic atom, aluminium or gallium, is tetrahedral. For an easier comparison of the structures, we listed relevant distances, bond lengths and angles in Table 2. The E···P distance for all adducts increases from oxygen-bridged **EOP** to sulphur-bridged **ESP** systems and from aluminium to gallium.

It is interesting to compare the structural parameters of the **EXP** adducts with those of the free **EXP** molecules. Similar to the examples of five-membered heterocyclic adducts of **AlOP**,[19,23,27] the E–X bonds are longer and the X–P bonds are shorter than in the free FLPs. For the E–X–P angle of the different adducts, the smallest changes are observed for the CS_2-adducts **EXP**·CS_2, while the carbon dioxide adducts **EXP**·CO_2 show the largest distortions.

While all atoms of the five-membered ring in the **EXP**·CO_2 and **EXP**·CS_2 adducts lie almost in the same plane (including the exocyclic atoms) the SO_2 adducts show a substantial

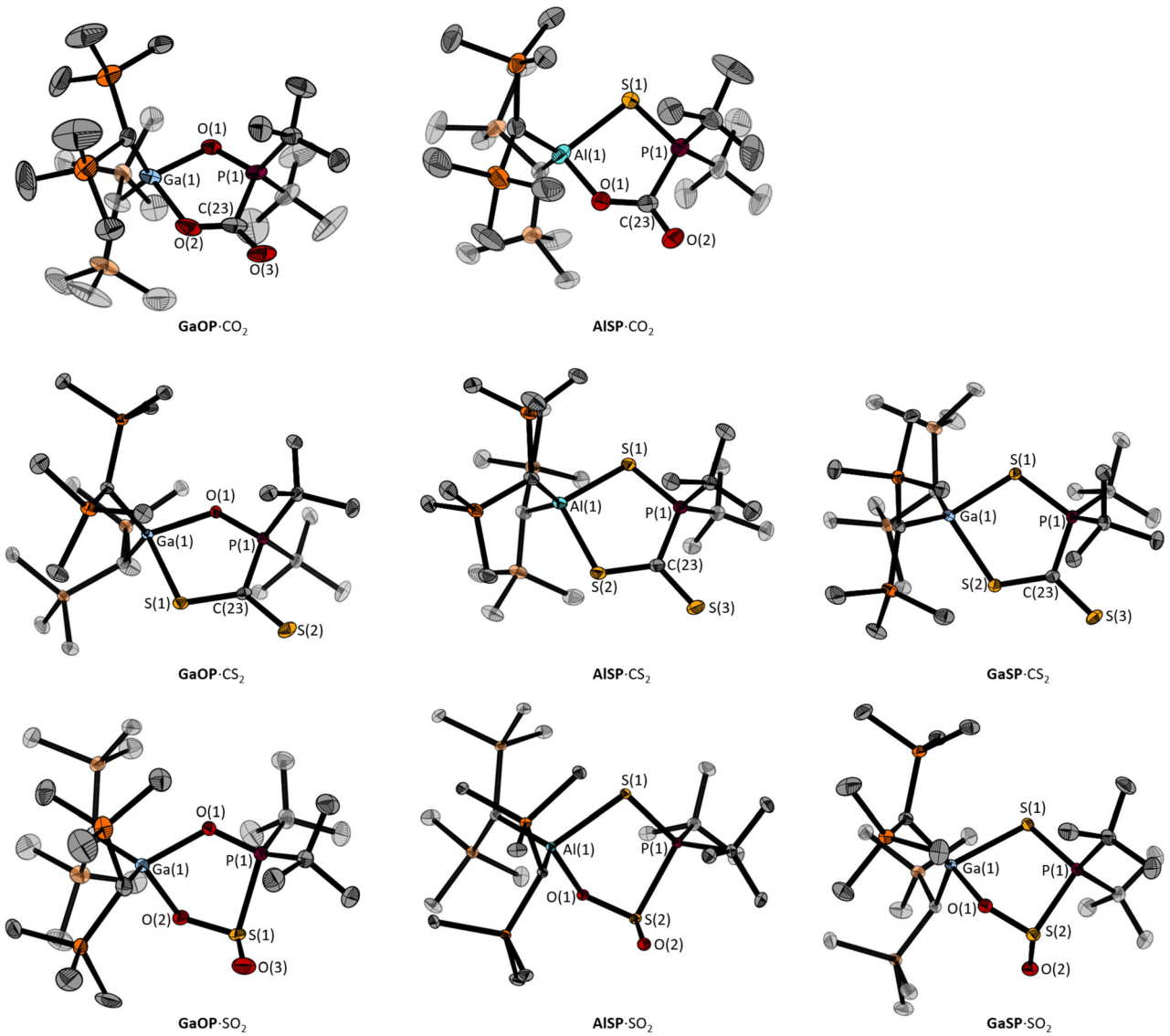

Fig. 4 Molecular structures of **GaOP**·CO_2, **GaOP**·CS_2, **GaOP**·SO_2, **AlSP**·CO_2, **AlSP**·CS_2, **AlSP**·SO_2, **GaSP**·CS_2, and **GaSP**·SO_2 in the solid state. Hydrogen atoms, solvent molecules, and minor occupied parts are omitted for clarity. Ellipsoids are set at 50% probability level.

Table 2 Selected bond lengths, distances and angles of the isolated **EXP**·CO_2, **EXP**·CS_2, and **EXP**·SO_2 adducts[23]

Compound	**AlOP**			**GaOP**			**AlSP**			**GaSP**		
Adduct	CO_2	CS_2	SO_2	CO_2	CS_2	SO_2	CO_2	CS_2	SO_2	CO_2	CS_2	SO_2
d(E···P)/Å	2.901(2)	3.033(1)	—	3.005(1)	3.116(1)	3.095(1)	3.255(1)	3.465(1)	3.427(1)	—	3.513(1)	3.481(1)
d(E–X)/Å	1.855(2)	1.827(1)	—	1.989(2)	1.959(1)	1.981(1)	2.477(2)	2.336(1)	2.414(1)	—	2.383(1)	2.451(1)
d(X–P)/Å	1.540(2)	1.544(1)	—	1.537(2)	1.532(1)	1.536(1)	1.979(2)	2.017(1)	2.008(1)	—	2.015(1)	2.007(1)
E–X–P/°	117.1(1)	128.0(1)	—	116.4(1)	126.0(1)	122.8(1)	93.2(1)	105.3(1)	101.2(1)	—	105.8(1)	102.2(1)
C–E–C/°	108.8(2)	119.6(1)	—	131.2(2)	123.8(1)	125.0(1)	123.3(1)	122.4(1)	123.0(1)	—	125.2(1)	127.3(1)

distortion from planarity. As expected, due to the presence of the lone electron pair at the sulphur atom, the oxygen atom bound to the aluminium or gallium atom, respectively, as well as the exocyclic oxygen atom deviate from this plane.

Further attempts to generate strained four-membered rings by transferring single oxygen or sulphur atoms were conducted using nitrogen oxide (N_2O) and propylene sulphide, respectively (Scheme 5). Interestingly, the **EXP** FLPs show different

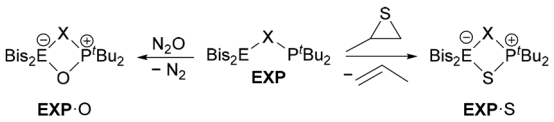

Scheme 5 Transfer of oxygen- and sulphur atoms by reaction of **EXP** with nitrogen dioxide and propylene sulphide under the loss of nitrogen and propene, respectively.

behaviours for the reaction with N_2O. Accompanying with the release of molecular nitrogen, the formal oxygen adducts $Bis_2GaOP^tBu_2$·O (**GaOP**·O) and $Bis_2AlSP^tBu_2$·O (**AlSP**·O) were formed, while **GaSP** showed no reaction even after heating to 70 °C for several days. ^{1}H NMR spectroscopic analyses showed similar high-field shifts for the *tert*-butyl groups and the methine protons in comparison to **EXP** for both oxygen adducts. The singlets in the $^{31}P\{^1H\}$ NMR spectra at 85.2 (**GaOP**·O) and 116.4 ppm (**AlSP**·O) also suggest a cooperative bonding of the oxygen atom by the LA and the LB function. For **AlSP**·O the four-membered heterocyclic motif was verified by X-ray diffraction measurements (Fig. 5). However, due to the limited quality of the crystals, only the connectivity can be discussed.

Previously reported by Uhl *et al.*, the formation of a sulphide adduct of a benzylidene bridged Ga/P FLP was achieved using propylene sulphide under the release of propene when heated.[28] In analogy, propylene sulphide and **GaOP** led to the formation of propene and the corresponding sulphide adduct $Bis_2GaOP^tBu_2$·S (**GaOP**·S) upon heating to 80 °C. The signals of **GaOP**·S in the ^{1}H NMR spectrum are slightly shifted towards higher field compared to those of **GaOP**·O. In contrast, the ^{31}P NMR signal of **GaOP**·S at 117.8 ppm is extremely broad, significantly shifted towards lower field and is between the ones of the free FLPs **GaOP** (143.5 ppm) and **GaSP** (68.5 ppm). Although the **GaSP** system reacts in an unselective way with N_2O, the reaction with propylene sulphide afforded $Bis_2GaSP^tBu_2$·S (**GaSP**·S) and it was possible to determine its molecular structure in the solid-state, by picking crystals, suitable for X-ray diffraction measurements, from the concentrated solution (Fig. 5).

Table 3 Overview of products resulting from the reaction of **EXP** with N_2O and propylene sulphide

	GaOP	AlSP	GaSP
N_2O	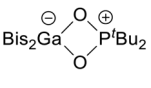 **GaOP**·O	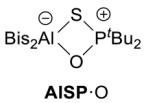 **AlSP**·O	No reaction
	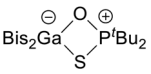 **GaOP**·S	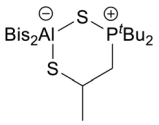 **AlSP**·SC_3H_6	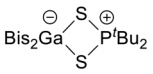 **GaSP**·S

Interestingly, the **AlSP** system showed a different behaviour (Table 3). In this case, a ring opening of propylene sulphide leads to the formation of a six-membered heterocycle without the outgassing of propene, despite heating to 80 °C. The connectivity was enlightened with the help of NMR spectroscopy: the aluminium atom binds to the sulphur atom, while the methylene unit is linked to the phosphorus atom. In the ^{1}H NMR spectrum the protons of the CH_2 unit are diastereotopic and therefore induce two different multiplets (1.62/1.82 ppm). Additionally, the multiplet at 3.12 ppm belongs to the methine proton of the propylene unit, as it is the case for the methyl-group at 1.46 ppm. The methine protons of the Bis-groups are detected at −0.54 ppm. Likewise to the adduct **AlSP**·SO_2, the *tert*-butyl resonance is split into two doublets at 0.80/0.91 ppm with $^3J_{P,H}$-couplings constants of 15.3/16.0 Hz. The ^{31}P NMR spectrum displays a broad singlet at 77.3 ppm.

The molecular structure in the solid-state of **AlSP**·SC_3H_6 validates the six-membered heterocycle. With 3.707(1) Å the Al···P distance is significantly larger than in the above-mentioned adducts of **AlSP**. The Al–S–P angle is also the widest with 112.2(1)°, probably resulting from the lower ring strain. The exact opposite trends are observed for the **GaSP**·S system: the Ga···P distance (3.034(2) Å) as well as the Ga–S–P angles (85.2(9)°) are drastically smaller than in the free **GaSP** (3.482(1) Å; 106.1(1)°).

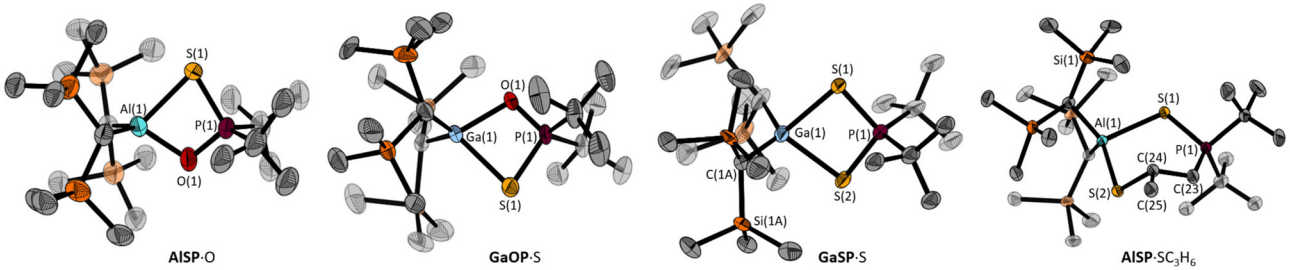

Fig. 5 Molecular structures of **AlSP**·O, **GaOP**·S, **GaSP**·S, and **AlSP**·SC_3H_6 in the solid-state. Hydrogen atoms and minor occupied parts are omitted for clarity. Ellipsoids are set at 50% probability level. Selected distances, bond lengths [Å] and angles [°]: **GaSP**·S: Ga(1)···P(1) 3.034(2), Ga(1)–S(1) 2.433(2), Ga(1)–S(2) 2.441(2), S(1)–P(1) 2.033(3), S(2)–P(1) 2.018(3); Ga(1)–S(1)–P(1) 85.1(1), Ga(1)–S(2)–P(1) 85.2(1), C(1A)–Ga(1)–C(8A) 122.3(6), S(1)–Ga(1)–S(2) 83.4(1), S(1)–P(1)–S(2) 106.3(1); **AlSP**·SC_3H_6: Al(1)···P(1) 3.707(1), Al(1)–S(1) 2.433(1), Al(1)–S(2) 2.272(1), S(1)–P(1) 2.025(1); Al(1)–S(1)–P(1) 112.2(1), C(1)–Al(1)–C(8) 117.1(1), S(1)–Al(1)–S(2) 99.2(1).

Conclusions

We expanded the range of geminal Al/P and Ga/P FLPs with the synthesis and full characterisation of the sulphur-bridged FLPs $Bis_2ESP^tBu_2$ (**ESP**, E = Al, Ga). In contrast to the oxygen-bridged systems **EOP**, no H_2 activation is observed for **ESP**. Likewise, no formal HBr adduct is formed for the **GaSP** FLP in the synthetic procedure, whereas **AlSP**·HBr was isolated and the molecular structure in the solid-state shows a stabilising intramolecular H···Br contact. According to the HSAB concept, a selective exchange reaction of **AlSP** and **GaOP** leads to **AlOP** and **GaSP**.

In combination with the oxygen-bridged **GaOP** system, the reactivity of sulphur-bridged **ESP** FLPs towards a series of small molecules (CO_2, CS_2, SO_2, N_2O, propylene sulphide) was tested. As expected, the adducts **EXP**·CO_2, **EXP**·CS_2, and **EXP**·SO_2 (X = O, S) comprise five-membered rings, and the reaction with N_2O results in the oxygen adduct **EXP**·O, with a four-membered heterocycle. The **GaSP** FLP is an exception and shows slightly different reactivity: a temperature-dependent CO_2 adduct, two structural isomers for **GaSP**·CS_2 and no reaction with N_2O.

The interesting colouration of the **EXP**·CS_2 adducts were analysed by UV/vis spectroscopy supported by quantum chemical calculations, which suggests that mainly the HOMO → LUMO transition produces the colouring. Furthermore, activation of propylene sulphide results in different adducts, for both gallium FLPs into the sulphide adduct **GaXP**·S with outgassing of propene. On the other hand, **AlSP** forms the addition product, a six-membered heterocycle.

This comparative study demonstrates how minor changes in Lewis acidity and basicity, involving different elements and linker units in intramolecular FLPs, affect reactivity, particularly with regard to the HSAB concept.

Experimental section

General methods

All reactions and manipulations with air and moisture sensitive compounds were carried out under conventional Schlenk techniques or in a glove box using argon as inert gas. Volatile compounds were handled in a vacuum line. The solvents *n*-hexane, toluene, toluene-d_8 and benzene-d_6 were dried over a Na/K alloy, dichloromethane over CaH_2, and were also distilled and degassed prior to use. Bis_2AlH,[1] Bis_2GaBr,[2] $Bis_2GaOP^tBu_2$,[2] and $^tBu_2P(S)H$[3] were prepared according to literature procedures. CO_2 (99.5%, Linde), SO_2 (99.98%, Air Liquid), and N_2O (extracted from a capsule for cream whipping) were used without further purification. CS_2 (99.9%, J.T. Baker) was dried over P_4O_{10}, distilled and degassed prior to use. Propylene sulphide (98%, TCI) was distilled and degassed prior to use. NMR spectra were recorded using a Bruker Avance III 500, Avance III 500 HD, Ascend 500 neo2K or Ascend 500 neo3K spectrometer at ambient temperature unless otherwise stated. Chemical shifts were referenced to the residual proton or carbon signal of the solvent (benzene-d_6: ^{1}H: 7.16 ppm, ^{13}C: 128.1 ppm; toluene-d_8: ^{1}H: 2.09 ppm) or externally (^{29}Si: $SiMe_4$, ^{31}P: 85% H_3PO_4 in H_2O). Elemental analyses were carried out using a HEKATECH EURO Elemental Analyzer.

Synthetic procedures

$^tBu_2P(S)H$. In an ampoule fitted with a greaseless tap, $^tBu_2PCl$ (1.14 g, 6.31 mmol) was dissolved in toluene (5 mL), degassed and pressurised with H_2S (1022 mbar, 16.5 mmol). After stirring for 8 d at 100 °C all volatiles were removed under reduced pressure. The residue was dissolved in dichloromethane (15 mL) and dried *in vacuo* again. *Via* sublimation (60 °C, 0.02 mbar) $^tBu_2P(S)H$ was isolated as a fluffy colourless solid (709 mg, 4.00 mmol, 63%). ^{1}H NMR (500 MHz, C_6D_6): δ [ppm] = 1.04 (d, $^3J_{P,H}$ = 16.2 Hz, 18H, C**H**$_3$), 5.51 (d, $^1J_{P,H}$ = 414.7 Hz, 1H, P**H**). $^{13}C\{^1H\}$ NMR (126 MHz, C_6D_6): δ [ppm] = 27.3 (s, C(**C**H$_3$)$_3$), 35.6 (d, $^1J_{P,C}$ = 42.7 Hz, **C**(CH$_3$)$_3$). $^{31}P\{^1H\}$ NMR (202 MHz, C_6D_6): δ [ppm] = 74.2 (s).

$Bis_2AlSP^tBu_2$ (AlSP). $^tBu_2P(S)H$ (189 mg, 1.06 mmol) was dissolved in *n*-hexane (10 mL) and added to a solution of Bis_2AlH (368 mg, 1.06 mmol) in *n*-hexane (10 mL), observing gas formation. After stirring for 1 h, all volatiles were removed under reduced pressure and the residue dried *in vacuo*. **AlSP** was obtained as a colourless crystalline solid (555 mg, 1.06 mmol, quant.). ^{1}H NMR (500 MHz, C_6D_6): δ [ppm] = 0.27 (s, 2H, AlC**H**), 0.34 (s, 36H, Si(C**H**$_3$)$_3$), 1.24 (d, $^3J_{P,H}$ = 11.6 Hz, 18H, C(C**H**$_3$)$_3$). $^{13}C\{^1H\}$ NMR (126 MHz, C_6D_6): δ [ppm] = 4.6 (s, Si(**C**H$_3$)$_3$), 10.5 (s, Al**C**H), 29.8 (d, $^2J_{P,C}$ = 15.4 Hz, C(**C**H$_3$)$_3$), 34.9 (d, $^1J_{P,C}$ = 34.3 Hz, **C**(CH$_3$)$_3$). $^{29}Si\{^1H\}$ NMR (99 MHz, C_6D_6): δ [ppm] = −3.3 (s). $^{31}P\{^1H\}$ NMR (202 MHz, C_6D_6): δ [ppm] = 69.2 (s). Elemental analysis calcd (%) for $C_{22}H_{56}AlPSSi_4$ (M_r = 523.05): C 50.52, H 10.79, S 6.13; found C 49.88, H 10.76, S 6.09.

$Bis_2GaSP(^tBu)_2$ (GaSP). $(^tBu)_2P(S)H$ (467 mg, 2.62 mmol) and Bis_2GaBr (1.240 g, 2.65 mmol) were dissolved in *n*-hexane (15 mL). Potassium hexamethyldisilazanide (539 mg, 2.70 mmol) was added as a solid in portions over 30 min. The milky suspension was stirred for 1 h, then filtered and all volatiles were removed under reduced pressure. The residue was dried under reduced pressure. **GaSP** was obtained as a colourless crystalline solid (1.417 g, 2.50 mmol, 96%). ^{1}H NMR (500 MHz, C_6D_6): δ [ppm] = 0.32 (s, 36H, Si(C**H**$_3$)$_3$), 1.06 (s, 2H, GaC**H**), 1.27 (d, $^3J_{P,H}$ = 11.5 Hz, 18H, C(C**H**$_3$)$_3$). $^{13}C\{^1H\}$ NMR (126 MHz, C_6D_6): δ [ppm] = 4.2 (s, Si(**C**H$_3$)$_3$), 18.3 (s, Ga**C**H), 30.0 (d, $^2J_{P,C}$ = 15.7 Hz, C(**C**H$_3$)$_3$), 34.9 (d, $^1J_{P,C}$ = 33.8 Hz, **C**(CH$_3$)$_3$). $^{29}Si\{^1H\}$ NMR (99 MHz, C_6D_6): δ [ppm] = −2.8 (s). $^{31}P\{^1H\}$ NMR (202 MHz, C_6D_6): δ [ppm] = 68.5 (s). Elemental analysis calcd (%) for $C_{22}H_{56}GaPSSi_4$ (M_r = 565.79): C 46.86, H 10.12, S 5.88; found C 46.70, H 9.98, S 5.67.

$Bis_2AlSP^tBu_2$·HBr (AlSP·HBr). $^tBu_2P(S)H$ (16 mg, 90 μmol) was dissolved in toluene (2 mL) and added to Bis_2AlBr (38 mg, 90 μmol). After stirring for 1 h, all volatiles were removed under reduced pressure and **AlSP**·HBr was isolated as a colourless solid (54 mg, 90 μmol, quant.). Crystals of **AlSP**·HBr suitable for X-ray diffraction were obtained by slow evaporation of a solution in C_6D_6. ^{1}H NMR (500 MHz, C_6D_6): δ [ppm] = −0.41

(s, 2H, AlC**H**), 0.45 (s, 36H, Si(C**H**$_3$)$_3$), 0.91 (d, $^3J_{P,H}$ = 17.2 Hz, 18H, C**H**$_3$), 6.02 (d, $^1J_{P,H}$ = 444.8 Hz, 1H, P**H**). ^{13}C{^{1}H} NMR (126 MHz, C_6D_6): δ [ppm] = 5.0 (s, Si(**C**H$_3$)$_3$), 8.9 (s, Al**C**H), 27.6 (d, $^2J_{P,C}$ = 2.3 Hz, C(**C**H$_3$)$_3$), 35.9 (d, $^1J_{P,C}$ = 39.3 Hz, **C**(CH$_3$)$_3$). ^{29}Si{^{1}H} NMR (99 MHz, C_6D_6): δ [ppm] = −1.8 (s). ^{31}P{^{1}H} NMR (121 MHz, C_6D_6): δ [ppm] = 69.7 (s). Elemental analysis calcd (%) for $C_{22}H_{57}BrAlSPSi_4$ (M_r = 587.90): C 43.75, H 9.51, S 5.31; found C 43.34, H 9.52, S 5.65.

Procedure for the CO_2 adducts Bis$_2$EXP^{t}Bu$_2$·CO_2 (EXP·CO_2). **EXP** was dissolved in *n*-hexane (4 mL), degassed (3 × freeze–pump–thaw) and pressurised with an atmosphere of carbon dioxide (1 atm.). After stirring for 24 h, all volatiles were removed under reduced pressure and the residue dried *in vacuo*. Crystals of **GaOP**·CO_2 and **AlSP**·CO_2 suitable for X-ray diffraction were obtained by slow evaporation of a solution in C_6D_6.

Bis$_2$GaOP^{t}Bu$_2$·CO_2 (**GaOP**·CO_2) was obtained as a colourless solid (42 mg, 71 μmol, quant.). ^{1}H NMR (500 MHz, C_6D_6): δ [ppm] = −0.35 (s, 2H, GaC**H**), 0.37 (s, 18H, Si(C**H**$_3$)$_3$), 0.39 (s, 18H, Si(C**H**$_3$)$_3$), 1.06 (d, $^3J_{P,H}$ = 15.1 Hz, 18H, C(C**H**$_3$)$_3$). ^{13}C{^{1}H} NMR (126 MHz, C_6D_6): δ [ppm] = 4.6 (s, Si(**C**H$_3$)$_3$), 4.8 (s, Ga**C**H), 26.7 (s, C(**C**H$_3$)$_3$), 34.7 (d, $^1J_{P,C}$ = 45.4 Hz, **C**(CH$_3$)$_3$), 167.2 (d, $^1J_{P,C}$ = 98.5 Hz, P**C**O$_2$). ^{29}Si{^{1}H} NMR (99 MHz, C_6D_6): δ [ppm] = −1.2 (s). ^{31}P{^{1}H} NMR (202 MHz, C_6D_6): δ [ppm] = 57.1 (s). Elemental analysis calcd (%) for $C_{23}H_{56}GaO_3PSi_4$ (M_r = 593.73): C 46.53, H 9.51; found C 46.30, H 9.78.

Bis$_2$AlSP^{t}Bu$_2$·CO_2 (**AlSP**·CO_2) was obtained as a colourless solid (39 mg, 69 μmol, quant.). ^{1}H NMR (500 MHz, C_6D_6): δ [ppm] = −0.79 (s, 2H, AlC**H**), 0.41 (s, 18H, Si(C**H**$_3$)$_3$), 0.42 (s, 18H, Si(C**H**$_3$)$_3$), 1.05 (d, $^3J_{P,H}$ = 16.8 Hz, 18H, C(C**H**$_3$)$_3$). ^{13}C{^{1}H} NMR (126 MHz, C_6D_6): δ [ppm] = 5.1 (s, Si(**C**H$_3$)$_3$), 5.3 (s, Si(**C**H$_3$)$_3$), 5.7 (s, Al**C**H), 27.3 (s, C(**C**H$_3$)$_3$), 38.3 (d, $^1J_{P,C}$ = 26.4 Hz, **C**(CH$_3$)$_3$), 163.3 (d, $^1J_{P,C}$ = 79.0 Hz, P**C**O$_2$). ^{29}Si{^{1}H} NMR (99 MHz, C_6D_6): δ [ppm] = −1.7 (s), −1.3 (s). ^{31}P{^{1}H} NMR (202 MHz, C_6D_6): δ [ppm] = 73.3 (s). Elemental analysis calcd (%) for $C_{23}H_{56}AlO_2PSSi_4$ (M_r = 567.05): C 48.72, H 9.95, S 5.65; found C 48.93, H 10.23, S 5.48.

Bis$_2$GaSP^{t}Bu$_2$·CO_2 (**GaSP**·CO_2): **GaSP** forms a temperature-dependent equilibrium with **GaSP**·CO_2 under an atmosphere of CO_2. VT NMR studies were conducted in the range between 253–373 K. ^{1}H NMR (500 MHz, C_6D_6): δ [ppm] = −0.27 (s, 2H, GaC**H**), 0.40 (s, 36H, Si(C**H**$_3$)$_3$), 1.13 (d, $^3J_{P,H}$ = 16.4 Hz, 18H, C(C**H**$_3$)$_3$). ^{13}C{^{1}H} NMR (126 MHz, C_6D_6): δ [ppm] = 4.9 (s, Si(**C**H$_3$)$_3$), 11.8 (s, Ga**C**H), 27.6 (s, C(**C**H$_3$)$_3$), 38.1 (d, $^1J_{P,C}$ = 27.0 Hz, **C**(CH$_3$)$_3$), 164.2 (d, $^1J_{P,C}$ = 75.1 Hz, P**C**O$_2$). ^{29}Si{^{1}H} NMR (99 MHz, C_6D_6): δ [ppm] = −0.6 (s). ^{31}P{^{1}H} NMR (202 MHz, C_6D_6): δ [ppm] = 67.9 (s).

Procedure for the CS_2 adducts Bis$_2$EXP^{t}Bu$_2$·CS_2 (EXP·CS_2). **EXP** was dissolved in *n*-hexane (3 mL) carbon disulfide (excess) was added, and the solutions show colourations within 5 min for **GaOP**·CS_2 (blue) and **AlSP**·CS_2 (green). For **GaSP**·CS_2 the reaction was slower and within 24 h a deep yellow colouration resulted. After stirring for 48 h, all volatiles were removed under reduced pressure and the residue dried *in vacuo*. Recrystallisation from *n*-hexane gave violet crystals in all cases.

Bis$_2$GaOP^{t}Bu$_2$·CS_2 (**GaOP**·CS_2) crystallises as wide, violet needles (11 mg, 18 μmol, 31%) from a concentrated *n*-hexane solution at −18 °C. ^{1}H NMR (500 MHz, C_6D_6): δ [ppm] = −0.17 (s, 2H, GaCH), 0.36 (s, 36H, Si(CH$_3$)$_3$), 1.14 (d, $^3J_{P,H}$ = 14.9 Hz, 18H, C(CH$_3$)$_3$). ^{13}C{^{1}H} NMR (126 MHz, C_6D_6): δ [ppm] = 4.7 (s, Si(CH$_3$)$_3$), 4.8 (s, Si(CH$_3$)$_3$), 11.4 (s, GaCH), 27.3 (s, C(CH$_3$)$_3$), 36.6 (d, $^1J_{P,C}$ = 51.0 Hz, C(CH$_3$)$_3$), 237.8 (d, $^1J_{P,C}$ = 42.4 Hz, PCS$_2$). ^{29}Si{^{1}H} NMR (99 MHz, C_6D_6): δ [ppm] = −1.5 (s), −0.9 (s). ^{31}P{^{1}H} NMR (202 MHz, C_6D_6): δ [ppm] = 63.5 (s). Elemental analysis calcd (%) for $C_{23}H_{56}GaOPS_2Si_4$ (M_r = 625.86): C 44.14, H 9.02, S 10.25; found C 44.35, H 8.93, S 10.17.

Bis$_2$AlSP^{t}Bu$_2$·CS_2 (**AlSP**·CS_2) crystallises as small violet blocks (22 mg, 37 μmol, 47%) from a concentrated *n*-hexane solution at −18 °C. ^{1}H NMR (500 MHz, C_6D_6): δ [ppm] = −0.59 (s, 2H, AlCH), 0.40 (s, 18H, Si(CH$_3$)$_3$), 0.42 (s, 18H, Si(CH$_3$)$_3$), 1.14 (d, $^3J_{P,H}$ = 16.5 Hz, 18H, C(CH$_3$)$_3$). ^{13}C{^{1}H} NMR (126 MHz, C_6D_6): δ [ppm] = 5.5 (s, Si(CH$_3$)$_3$), 7.0 (s, AlCH), 28.4 (s, C(CH$_3$)$_3$), 41.7 (d, $^1J_{P,C}$ = 29.5 Hz, C(CH$_3$)$_3$), 232.7 (d, $^1J_{P,C}$ = 18.3 Hz, PCS$_2$). ^{29}Si{^{1}H} NMR (99 MHz, C_6D_6): δ [ppm] = −1.5 (s), −1.4 (s). ^{31}P{^{1}H} NMR (202 MHz, C_6D_6): δ [ppm] = 91.9 (s). Elemental analysis calcd (%) for $C_{23}H_{56}AlPS_3Si_4$ (M_r = 599.18): C 46.11, H 9.42, S 16.05; found C 46.44, H 9.80, S 15.69.

Bis$_2$GaSP^{t}Bu$_2$·CS_2 (**GaSP**·CS_2) crystallises as small violet blocks (56 mg, 87 μmol, 46%) from a concentrated *n*-hexane solution at −18 °C. 'Classical' adduct (**GaSCP**-connectivity): ^{1}H NMR (500 MHz, C_6D_6): δ [ppm] = −0.12 (s, 2H, GaCH), 0.38 (s, 18H, Si(CH$_3$)$_3$), 0.39 (s, 18H, Si(CH$_3$)$_3$), 1.19 (d, $^3J_{P,H}$ = 16.3 Hz, 18H, C(CH$_3$)$_3$). ^{13}C{^{1}H} NMR (126 MHz, C_6D_6): δ [ppm] = 5.0 (s, Si(CH$_3$)$_3$), 5.1 (s, Si(CH$_3$)$_3$), 12.6 (s, GaCH), 28.6 (s, C(CH$_3$)$_3$), 41.7 (d, $^1J_{P,C}$ = 30.1 Hz, C(CH$_3$)$_3$), 233.0 (d, $^1J_{P,C}$ = 16.2 Hz, PCS$_2$). ^{29}Si{^{1}H} NMR (99 MHz, C_6D_6): δ [ppm] = −0.6 (s), −0.5 (s). ^{31}P{^{1}H} NMR (202 MHz, C_6D_6): δ [ppm] = 91.7 (s). 'Inverted' adduct (**GaCSP**-connectivity): ^{1}H NMR (500 MHz, C_6D_6): δ [ppm] = −0.13 (s, 2H, GaC**H**), 0.24 (s, 36H, Si(C**H**$_3$)$_3$), 1.44 (d, $^3J_{P,H}$ = 16.0 Hz, 18H, C(C**H**$_3$)$_3$). ^{13}C{^{1}H} NMR (126 MHz, C_6D_6): δ [ppm] = 4.2 (s, Si(**C**H$_3$)$_3$), 13.2 (s, Ga**C**H), 28.6 (s, C(**C**H$_3$)$_3$), 40.7 (d, $^1J_{P,C}$ = 36.4 Hz, **C**(CH$_3$)$_3$), 255.8 (s, Ga**C**S$_2$). ^{29}Si{^{1}H} NMR (99 MHz, C_6D_6): δ [ppm] = −0.3 (s). ^{31}P{^{1}H} NMR (202 MHz, C_6D_6): δ [ppm] = 97.1 (s). Elemental analysis calcd (%) for $C_{23}H_{56}GaPS_3Si_4$ (M_r = 641.92): C 43.04, H 8.79, S 14.98; found C 43.28, H 9.05, S 14.87.

Procedure for Bis$_2$EXP^{t}Bu$_2$·SO_2 (EXP·SO_2). **EXP** was dissolved in *n*-hexane (3 mL), degassed (3× feeze–pump–thaw) and SO_2 (excess) was condensed onto the frozen solution. After stirring for 24 h, all volatiles were removed under reduced pressure and the residue dried *in vacuo*. **EXP**·SO_2 were obtained as colourless solids. Crystals of **EXP**·SO_2 suitable for X-ray diffraction were obtained by slow evaporation of a solution in C_6D_6.

Bis$_2$GaOP^{t}Bu$_2$·SO_2 (**GaOP**·SO_2) was obtained as a colourless solid (23 mg, 38 μmol, quant.). ^{1}H NMR (500 MHz, C_6D_6): δ [ppm] = −0.31 (br. s, 1H, GaC**H**), −0.03 (br. s, 1H, GaC**H**), 0.37–0.49 (m, 36H, Si(C**H**$_3$)$_3$), 0.87 (d, $^3J_{P,H}$ = 14.5 Hz, 9H, C(C**H**$_3$)$_3$), 1.21 (d, $^3J_{P,H}$ = 15.1 Hz, 9H, C(C**H**$_3$)$_3$). ^{13}C{^{1}H} NMR (126 MHz, C_6D_6): δ [ppm] = 4.8 (s, Si(**C**H$_3$)$_3$), 5.0 (s, Si(**C**H$_3$)$_3$), 12.2 (br. s, Ga**C**H), 26.7 (s, C(**C**H$_3$)$_3$), 27.1 (s, C(**C**H$_3$)$_3$), 37.0 (d, $^1J_{P,C}$ = 21.1 Hz, **C**(CH$_3$)$_3$), 39.3 (d, $^1J_{P,C}$ = 21.2 Hz, **C**(CH$_3$)$_3$). ^{29}Si{^{1}H} NMR (99 MHz, C_6D_6): δ [ppm] = −1.3 (s), −0.9 (s). ^{31}P{^{1}H}

NMR (202 MHz, C_6D_6): δ [ppm] = 88.1 (s). Elemental analysis calcd (%) for $C_{22}H_{56}GaO_3PSSi_4$ (M_r = 613.78): C 43.05, H 9.20, S 5.22; found C 42.51, H 9.03, S 5.30.

Bis$_2$AlSP^{t}Bu$_2$·SO$_2$ (AlSP·SO$_2$) was obtained as a colourless solid (21 mg, 37 μmol, quant.). ^{1}H NMR (500 MHz, C_6D_6): δ [ppm] = −0.69 (br. s, 1H, AlC**H**), −0.57 (br. s, 1H, AlC**H**), 0.31–0.59 (m, 36H, Si(C**H**$_3$)$_3$), 0.89 (d, $^3J_{P,H}$ = 16.3 Hz, 9H, C(C**H**$_3$)$_3$), 1.18 (d, $^3J_{P,H}$ = 16.4 Hz, 9H, C(C**H**$_3$)$_3$). ^{13}C{^{1}H} NMR (126 MHz, C_6D_6): δ [ppm] = 5.0 (s, Si(**C**H$_3$)$_3$), 5.2 (s, Si(**C**H$_3$)$_3$), 6.1 (s, Al**C**H), 8.5 (s, Al**C**H), 27.5 (s, C(**C**H$_3$)$_3$), 27.9 (s, C(**C**H$_3$)$_3$), 39.2 (d, $^1J_{P,C}$ = 21.3 Hz, **C**(CH$_3$)$_3$), 42.4 (d, $^1J_{P,C}$ = 18.9 Hz, **C**(CH$_3$)$_3$). ^{29}Si{^{1}H} NMR (99 MHz, C_6D_6): δ [ppm] = −1.5 (s). ^{31}P{^{1}H} NMR (202 MHz, C_6D_6): δ [ppm] = 117.0 (s). Elemental analysis calcd (%) for $C_{22}H_{56}AlO_2PS_2Si_4$ (M_r = 587.10): C 45.01, H 9.61, S 10.92; found C 45.11, H 9.59, S 10.92.

Bis$_2$GaSP^{t}Bu$_2$·SO$_2$ (GaSP·SO$_2$) was obtained as a colourless solid (25 mg, 39 μmol, 95%). ^{1}H NMR (500 MHz, C_6D_6): δ [ppm] = −0.08 (br. s, 2H, GaC**H**), 0.44 (s, 36H, Si(C**H**$_3$)$_3$), 1.07 (br. s, 18H, C(C**H**$_3$)$_3$). ^{13}C{^{1}H} NMR (126 MHz, C_6D_6): δ [ppm] = 5.1 (s, Si(**C**H$_3$)$_3$), 28.3 (s, C(**C**H$_3$)$_3$), carbon atoms (Ga**C**H, **C**(CH$_3$)$_3$) not detected due to broadening. ^{29}Si{^{1}H} NMR (99 MHz, C_6D_6): δ [ppm] = −1.1 (s). ^{31}P{^{1}H} NMR (202 MHz, C_6D_6): δ [ppm] = 114.9 (s). Elemental analysis calcd (%) for $C_{23}H_{56}GaO_2PS_2Si_4$ (M_r = 629.84): C 41.95, H 8.96, S 10.18; found C 42.38, H 9.07, S 9.99.

Procedure for Bis$_2$EXP^{t}Bu$_2$·O (EXP·O). Bis$_2$EXP^{t}Bu$_2$ was dissolved in *n*-hexane (3 mL), degassed (3× freeze–pump–thaw) and N_2O (excess) was condensed onto the frozen solution. After stirring for 24 h, all volatiles were removed under reduced pressure and the residue dried *in vacuo*. **GaOP**·O (23 mg, 40 μmol, quant.) and **AlSP**·O (16 mg, 30 μmol, 92%) were obtained as colourless solids. **GaSP** shows no reaction with N_2O, even after heating to 70 °C. Crystals of **EXP**·O suitable for X-ray diffraction were obtained by slow evaporation of a solution in C_6D_6.

Bis$_2$GaOP^{t}Bu$_2$·O (GaOP·O) was obtained as a colourless solid (23 mg, 40 μmol, quant.). ^{1}H NMR (500 MHz, C_6D_6): δ [ppm] = 0.18 (s, 2H, GaC**H**), 0.38 (s, 36H, Si(C**H**$_3$)$_3$), 1.18 (d, $^3J_{P,H}$ = 14.0 Hz, 18H, C(C**H**$_3$)$_3$). ^{13}C{^{1}H} NMR (126 MHz, C_6D_6): δ [ppm] = 4.6 (s, Si(**C**H$_3$)$_3$), 13.3 (s, Ga**C**H), 27.5 (s, C(**C**H$_3$)$_3$), 35.7 (d, $^1J_{P,C}$ = 73.5 Hz, **C**(CH$_3$)$_3$). ^{29}Si{^{1}H} NMR (99 MHz, C_6D_6): δ [ppm] = −1.3 (s). ^{31}P{^{1}H} NMR (202 MHz, C_6D_6): δ [ppm] = 85.2 (s). Elemental analysis calcd (%) for $C_{22}H_{56}GaO_2PSi_4$ (M_r = 565.72): C 46.71, H 9.98; found C 46.76, H 10.13.

Bis$_2$AlSP^{t}Bu$_2$·O (AlSP·O) was obtained as a colourless solid (16 mg, 30 μmol, 92%). ^{1}H NMR (500 MHz, C_6D_6): δ [ppm] = −0.54 (br. s, 1H, AlC**H**), −0.47 (br. s, 1H, AlC**H**), 0.42 (s, 36H, Si(C**H**$_3$)$_3$), 1.09 (d, $^3J_{P,H}$ = 16.3 Hz, 18H, C(C**H**$_3$)$_3$). ^{13}C{^{1}H} NMR (126 MHz, C_6D_6): δ [ppm] = 5.1 (s, Si(**C**H$_3$)$_3$), 5.5 (s, Si(**C**H$_3$)$_3$), 9.5 (s, Al**C**H), 27.0 (d, $^2J_{P,C}$ = 2.8 Hz, C(**C**H$_3$)$_3$), 35.7 (d, $^1J_{P,C}$ = 50.1 Hz, **C**(CH$_3$)$_3$). ^{29}Si{^{1}H} NMR (99 MHz, C_6D_6): δ [ppm] = −2.0 (s). ^{31}P{^{1}H} NMR (202 MHz, C_6D_6): δ [ppm] = 116.4 (s). Elemental analysis calcd (%) for $C_{22}H_{56}AlOPSSi_4$ (M_r = 539.04): C 49.02, H 10.47, S 5.95; found C 49.20, H 10.64, S 5.83.

Bis$_2$GaOP^{t}Bu$_2$·S (GaOP·S). **GaOP** (96.1 mg, 0.17 mmol) was dissolved in toluene (3 mL), degassed (3× freeze–pump–thaw) and propylene sulphide (20 mbar, excess) was condensed onto the frozen solution. After stirring for 24 h at 80 °C, all volatiles were removed under reduced pressure and the residue dried *in vacuo*. **GaOP**·S was obtained as a colourless solid (79 mg, 0.14 mmol, 78%). Crystals of **GaOP**·S suitable for X-ray diffraction were obtained by slow evaporation of a solution in C_6D_6. ^{1}H NMR (500 MHz, C_6D_6): δ [ppm] = 0.22 (s, 2H, GaC**H**), 0.40 (s, 36H, Si(C**H**$_3$)$_3$), 1.17 (d, $^3J_{P,H}$ = 15.9 Hz, 18H, C(C**H**$_3$)$_3$). ^{13}C{^{1}H} NMR (126 MHz, C_6D_6): δ [ppm] = 4.6 (s, Si(**C**H$_3$)$_3$), Ga**C**H not detected, 27.4 (d, $^2J_{P,C}$ = 2.3 Hz, C(**C**H$_3$)$_3$), 39.6 (d, $^1J_{P,C}$ = 52.4 Hz, **C**(CH$_3$)$_3$). ^{29}Si{^{1}H} NMR (99 MHz, C_6D_6): δ [ppm] = −1.0 (s). ^{31}P{^{1}H} NMR (202 MHz, C_6D_6): δ [ppm] = 117.8 (br. s). Elemental analysis calcd (%) for $C_{22}H_{56}GaOPSSi_4$ (M_r = 581.79): C 45.42, H 9.70, S 5.51; found C 45.60, H 9.42 S 5.51.

Bis$_2$AlSP^{t}Bu$_2$·SC$_3$H$_6$ (AlSP·SC$_3$H$_6$). **AlSP** (32.0 mg, 61 μmol) was dissolved in toluene (3 mL), degassed (3× freeze–pump–thaw) and propylene sulphide (12 mbar, excess) was condensed onto the frozen solution. After stirring for 24 h at 80 °C, all volatiles were removed under reduced pressure and the residue dried *in vacuo*. **AlSP**·SC$_3$H$_6$ was obtained as a colourless solid (35 mg, 58 μmol, 95%). Crystals of **AlSP**·SC$_3$H$_6$ suitable for X-ray diffraction were obtained by slow evaporation of a solution in C_6D_6. ^{1}H NMR (500 MHz, C_6D_6): δ [ppm] = −0.54 (m, 2H, AlC**H**), 0.49–0.57 (m, 36H, Si(C**H**$_3$)$_3$), 0.80 (d, $^3J_{P,H}$ = 15.3 Hz, 9H, C(C**H**$_3$)$_3$), 0.91 (d, $^3J_{P,H}$ = 16.0 Hz, 9H, C(C**H**$_3$)$_3$), 1.46 (dd, 3H, C**H**$_3$), 1.62 (ddd, 1H, PC**H**$_2$), 1.82 (ddd, 1H, PC**H**$_2$), 3.12 (m, 1H, OC**H**). ^{13}C{^{1}H} NMR (126 MHz, C_6D_6): δ [ppm] = 5.3, 5.5, 5.6 (s, Si(**C**H$_3$)$_3$), 6.8 (s, Al**C**H), 26.7 (s, C(**C**H$_3$)$_3$), 27.1 (s, C(**C**H$_3$)$_3$), 28.9 (d, $^3J_{P,C}$ = 13.8 Hz, **C**H$_3$), 30.3 (d, $^1J_{P,C}$ = 40.0 Hz, **C**H$_2$), 31.4 (d, $^2J_{P,C}$ = 4.6 Hz, O**C**H), 37.6 (d, $^1J_{P,C}$ = 37.7 Hz, **C**(CH$_3$)$_3$), 38.7 (d, $^1J_{P,C}$ = 40.0 Hz, **C**(CH$_3$)$_3$). ^{29}Si{^{1}H} NMR (99 MHz, C_6D_6): δ [ppm] = −1.3 (s). ^{31}P{^{1}H} NMR (202 MHz, C_6D_6): δ [ppm] = 77.4 (s). Elemental analysis calcd (%) for $C_{25}H_{62}AlPS_2Si_4$ (M_r = 597.19): C 50.28, H 10.47, S 10.74; found C 50.08, H 10.36, S 11.08.

Author contributions

J. Buth: investigation, methodology, validation, visualisation, writing (original draft), Y. V. Vishnevskiy (quantum chemical calculations), J.-H. Lamm, B. Neumann, and H.-G. Stammler: investigation (SCXRD), N. W. Mitzel: funding acquisition, project administration, supervision, writing, reviewing and editing.

Conflicts of interest

There are no conflicts to declare.

Data availability

The data that supports the findings of this study are available in the supplementary information (SI). Supplementary infor-

mation: NMR spectra, crystallographic data and computational details. See DOI: https://doi.org/10.1039/d6dt00151c.

CCDC 2503479–2503493 contain the supplementary crystallographic data for this paper.[29a–o]

Acknowledgements

The authors thank Marco Wißbrock and Dr Andreas Mix for recording VT and DOSY NMR spectra, Barbara Teichner for performing elemental analyses, Erik Niekamp, Marvin Waschipki, Ece Ayhan, and Hannah Koch for support with syntheses.

This work was funded by the Deutsche Forschungsgemeinschaft (DFG, German Research Foundation, grant MI 477/44-1, project no. 461833739, and grant VI 713/3-1, project no. 243500032). We acknowledge support by the Paderborn Center for Parallel Computing (PC2, HPC system Noctua 2) and by the Regional Computing Centre of the University of Cologne (RRZK, HPC system RAMSES) for providing computing time.

References

1 R. G. Pearson, *J. Am. Chem. Soc.*, 1963, **85**, 3533–3539.
2 A. D. Pournara, J.-H. Tang, L. Yang, J.-T. Liu, X.-Y. Huang, M.-L. Feng and M. G. Kanatzidis, *Chem. Mater.*, 2024, **36**, 3013–3021.
3 D. W. Stephan, G. C. Welch, R. R. S. Juan and J. D. Masuda, *Science*, 2006, **314**, 1124–1126.
4 D. W. Stephan, *J. Am. Chem. Soc.*, 2015, **137**, 10018–10032.
5 D. W. Stephan, *Science*, 2016, **354**, aaf7229.
6 P. Spies, G. Erker, G. Kehr, K. Bergander, R. Fröhlich, S. Grimme and D. W. Stephan, *Chem. Commun.*, 2007, 5072.
7 G. C. Welch and D. W. Stephan, *J. Am. Chem. Soc.*, 2007, **129**, 1880–1881.
8 S. Styra, M. Radius, E. Moos, A. Bihlmeier and F. Breher, *Chem. –Eur. J.*, 2016, **22**, 9508–9512.
9 C. Appelt, H. Westenberg, F. Bertini, A. W. Ehlers, J. C. Slootweg, K. Lammertsma and W. Uhl, *Angew. Chem., Int. Ed.*, 2011, **50**, 3925–3928.
10 J. Possart and W. Uhl, *Organometallics*, 2018, **37**, 1314–1323.
11 K. Chang, X. Wang, Z. Fan and X. Xu, *Inorg. Chem.*, 2018, **57**, 8568–8580.
12 M. Pieper, J.-H. Lamm, B. Neumann, H.-G. Stammler and N. W. Mitzel, *Dalton Trans.*, 2017, **46**, 5326–5336.
13 B. Waerder, M. Pieper, L. A. Körte, T. A. Kinder, A. Mix, B. Neumann, H.-G. Stammler and N. W. Mitzel, *Angew. Chem., Int. Ed.*, 2015, **54**, 13416–13419.
14 P. Holtkamp, F. Friedrich, E. Stratmann, A. Mix, B. Neumann, H.-G. Stammler and N. W. Mitzel, *Angew. Chem., Int. Ed.*, 2019, **58**, 5114–5118.
15 F. Breher, F. Krämer, J. Paradies and I. Fernández, *Nat. Chem.*, 2024, **16**, 63–69.
16 J. Krieft, H. Koch, B. Neumann, H.-G. Stammler, J.-H. Lamm, A. Mix and N. W. Mitzel, *Dalton Trans.*, 2024, **53**, 16280–16286.
17 D. Zhu, Z.-W. Qu and D. W. Stephan, *Dalton Trans.*, 2020, **49**, 901–910.
18 Y. Wang, Z. H. Li and H. Wang, *RSC Adv.*, 2018, **8**, 26271–26276.
19 L. Wickemeyer, P. C. Trapp, N. Aders, B. Neumann, H. Stammler and N. W. Mitzel, *Chem. –Eur. J.*, 2023, **29**, e202203685.
20 W. Uhl, M. Willeke, F. Hengesbach, A. Hepp and M. Layh, *Organometallics*, 2016, **35**, 3701–3712.
21 W. Uhl, M. Willeke, A. Hepp, D. Pleschka and M. Layh, *Z. Anorg. Allg. Chem.*, 2017, **643**, 387–397.
22 J. Buth, M. J. Klingsiek, Y. V. Vishnevskiy, A. Mix, J.-H. Lamm, B. Neumann, H.-G. Stammler and N. W. Mitzel, *ChemistryEurope*, 2025, e20250030723.
23 L. Wickemeyer, N. Aders, A. Mix, B. Neumann, H.-G. Stammler, J. J. Cabrera-Trujillo, I. Fernández and N. W. Mitzel, *Chem. Sci.*, 2022, **13**, 8088–8094.
24 G. Y. Li and W. J. Marshall, *Organometallics*, 2002, **21**, 590–591.
25 S. Alvarez, *Dalton Trans.*, 2013, **42**, 8617.
26 G. R. Fulmer, A. J. M. Miller, N. H. Sherden, H. E. Gottlieb, A. Nudelman, B. M. Stoltz, J. E. Bercaw and K. I. Goldberg, *Organometallics*, 2010, **29**, 2176–2179.
27 L. Wickemeyer, L. Hartmann, B. Neumann, H. Stammler and N. W. Mitzel, *Chem. –Eur. J.*, 2023, **29**, e202202842.
28 W. Uhl, J. Possart, A. Hepp and M. Layh, *Z. Anorg. Allg. Chem.*, 2017, **643**, 1016–1029.
29 (*a*) CCDC 2503479: Experimental Crystal Structure Determination, 2026, DOI: 10.5517/ccdc.csd.cc2q12d8; (*b*) CCDC 2503480: Experimental Crystal Structure Determination, 2026, DOI: 10.5517/ccdc.csd.cc2q12f9; (*c*) CCDC 2503481: Experimental Crystal Structure Determination, 2026, DOI: 10.5517/ccdc.csd.cc2q12gb; (*d*) CCDC 2503482: Experimental Crystal Structure Determination, 2026, DOI: 10.5517/ccdc.csd.cc2q12hc; (*e*) CCDC 2503483: Experimental Crystal Structure Determination, 2026, DOI: 10.5517/ccdc.csd.cc2q12jd; (*f*) CCDC 2503484: Experimental Crystal Structure Determination, 2026, DOI: 10.5517/ccdc.csd.cc2q12kf; (*g*) CCDC 2503485: Experimental Crystal Structure Determination, 2026, DOI: 10.5517/ccdc.csd.cc2q12lg; (*h*) CCDC 2503486: Experimental Crystal Structure Determination, 2026, DOI: 10.5517/ccdc.csd.cc2q12mh; (*i*) CCDC 2503487: Experimental Crystal Structure Determination, 2026, DOI: 10.5517/ccdc.csd.cc2q12nj; (*j*) CCDC 2503488: Experimental Crystal Structure Determination, 2026, DOI: 10.5517/ccdc.csd.cc2q12pk; (*k*) CCDC 2503489: Experimental Crystal Structure Determination, 2026, DOI: 10.5517/ccdc.csd.cc2q12ql; (*l*) CCDC 2503490: Experimental Crystal Structure Determination, 2026, DOI: 10.5517/ccdc.csd.cc2q12rm;

(*m*) CCDC 2503491: Experimental Crystal Structure Determination, 2026, DOI: 10.5517/ccdc.csd.cc2q12sn; (*n*) CCDC 2503492: Experimental Crystal Structure Determination, 2026, DOI: 10.5517/ccdc.csd.cc2q12tp; (*o*) CCDC 2503493: Experimental Crystal Structure Determination, 2026, DOI: 10.5517/ccdc.csd.cc2q12vq.